



Failure Cause Analysis of High-Rise Residential Fire Alarms Based on Pyrosim Simulation

Tao Liu^{1,a}, Ye Chen^{1,b,*}, Jun Li^{1,c}, Shuogui Zeng^{1,d}, Fuwei He², Zhenxi Liu³

¹School of Mechanical Engineering, Sichuan University of Science & Engineering, No. 1, Baita Road, Sanjiang New Area, Yibin, Sichuan, China

²Luzhou Fire and Rescue department, Luzhou, Sichuan, China

³Yibin Fire and Rescue department, Yibin, Sichuan, China

^a2242991685@qq.com, ^{b*}cy32428yr@suse.edu.cn,

^c58501323@qq.com, ^d1187033047@qq.com

Abstract. High-rise residential fires pose a significant threat to the life and property safety of residents. To address the issue of inadequate early feature recognition by photoelectric smoke alarms in current high-rise residential buildings, this study employs FDS simulation software Pyrosim to establish a typical high-rise residential room model. The effects of ambient wind speed and monitoring point height on dimming rate, room temperature distribution, and CO concentration are analyzed to identify the causes of fire alarm failures. Results indicate that as ambient wind speed increases, the time required for dimming rate, temperature, and CO concentration monitoring values to reach the alarm threshold significantly increases. Specifically, when the ambient wind speed is 10 m/s, the alarm times increase by 4.8, 1.45, and 1.76 times, respectively, compared to no wind conditions, which substantially diminishes the early warning capability of fire alarms. The findings of this study provide valuable insights for enhancing the safety of high-rise residential buildings and improving multi-sensor fusion warning systems for fire alarms in such structures.

Keywords: fire alarm; high-rise residence; numerical simulation; ambient wind speed

1 Introduction

The rapid expansion of urban areas has driven the development of high-rise residential buildings, which play a crucial role in optimizing land resource utilization and enhancing spatial efficiency. However, their inherent characteristics, including vertical height, high population density, and substantial fire load, make them particularly vulnerable to severe losses in the event of a fire[1]. According to statistics from China's National Fire and Rescue Administration (January to August 2024), high-rise residential fires accounted for 36, 000 of the 660, 000 nationwide fire incidents, resulting in 203 fatalities,

which represents over 15% of total fire-related casualties. These data underscore the significant threat posed by high-rise residential fires to public safety and property.

Early fire detection and timely intervention in residential settings can significantly improve evacuation success rates and reduce property damage. Environmental factors, particularly wind fields, exert a substantial influence on fire behavior in high-rise buildings, with wind speed increasing with height following a power-law relationship [2]. Consequently, fires on upper floors are subject to more pronounced wind effects, which significantly impact fire development and spread. Song et al.[3] demonstrated that environmental wind accelerates horizontal fire spread along building facades, with the leeward side exhibiting the largest spread area. Yang et al.[4], using CFD software Fluent coupled with the Weather Research and Forecasting (WRF) model, found that both parallel and antiparallel wind directions promote horizontal and vertical flame spread in high-rise buildings. He et al.[5] conducted experiments on stairwell fire dynamics, showing that increasing wind speed reduces initial flame volume and the time required to reach stable combustion. Gao et al. [6] studied the impact of environmental wind on heat release rate (HRR) using mass loss calorimetry, revealing that HRR increases rapidly with wind speed when airflow is not directly aligned with the fire source, with HRR at 5 m/s being 1.8 times greater than at 0 m/s.

Photoelectric smoke detectors are widely used in residential fire warning systems due to their high safety, adaptability, low false alarm rate, and ease of maintenance. However, their design standards do not fully account for the interference of high-wind environments, and research on their reliability under such conditions remains limited. To evaluate the performance of photoelectric smoke detectors in high-rise residential fires, this study employs FDS simulation software Pyrosim to establish a typical residential room fire model. The model analyzes the effects of different wind speeds and vertical heights on light obscuration rate, temperature distribution, and CO concentration during a fire, as well as the time required for monitoring points to reach design thresholds. The results provide insights for improving fire safety in high-rise buildings and developing multi-sensor fusion early warning systems.

2 Research Process

2.1 Calculation Model

Fig. 1 presents the computational model schematic, with its detailed parameters listed in Table 1. As shown, the model represents a master bedroom in a residential setting with dimensions of 3.3 m (W) \times 5.8 m (L) \times 3 m (H), comprising both a bedroom and an attached bathroom to simulate realistic air flow and thermal comfort conditions. The window is designed as a sliding type with overall dimensions of 1.8 m (w) \times 1 m (h), divided into two sections, each measuring 0.5 m in width and 1 m in height. The model incorporates four types of furniture—a bed, wardrobe, bedside table, and storage cabinet—based on typical residential bedroom layouts.

In this paper, PyroSim, developed based on Fire Dynamics Simulator (FDS), was selected to simulate fires in the model. Based on the principles of conservation of mass,

momentum and energy, the spatial geometry of a typical house is divided into several small rectangular control units or computing units [7, 8].

Table 1. Model Parameters Table

Name	<i>H</i>	<i>W</i>	<i>L</i>	<i>w</i>	<i>h</i>
Numerical value (m)	3	3.3	5.8	1.8	1

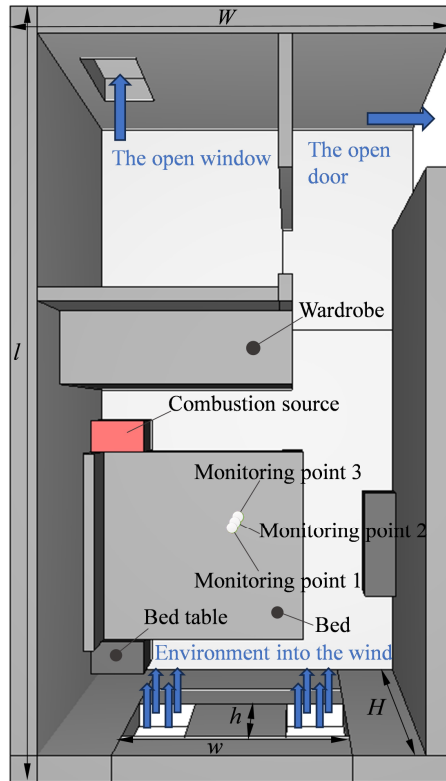


Fig. 1. Geometric model diagram

Mass conservation equation:

$$\frac{\partial \rho}{\partial t} + \nabla \cdot \rho u = 0 \tag{1}$$

Momentum conservation equation:

$$\rho \left(\frac{\partial u}{\partial t} + (u \nabla) u \right) + \nabla p = \rho g + f + \nabla \tau \tag{2}$$

Energy conservation equation :

$$\frac{\partial}{\partial t}(\rho h) + \nabla \cdot \rho h u = \frac{Dp}{Dt} + \dot{q}''' - \dot{q}_b''' - \nabla \cdot \dot{q}'' + \varepsilon \quad (3)$$

Where ρ is the density, kg/m³; ∇ is the Hamiltonian operator; u is the velocity vector, m/s; t is the time, s; p is the pressure, Pa; g is the gravitational acceleration, m/s²; f is the external force vector acting on the fluid, kg/(s²·m); τ is the viscous force tensor, kg/(s²·m); h is the specific enthalpy, J/kg; D is the diffusion coefficient, m²/s; \dot{q}''' is the heat release rate per unit volume, kW/m³; \dot{q}_b''' is the energy transmitted to the evaporating droplets, kJ; \dot{q}'' is the conduction heat and radiant heat, kW/m²; ε is the dissipative function.

The average wind speed of the ambient wind field at each height can be calculated according to the power empirical formula [2] :

$$u_z = u_1 \left(z / z_1 \right)^n \quad (4)$$

u_z is the estimated average wind speed at height z , m/s; u_1 is the average wind speed at a known altitude, m/s; n is the ground roughness coefficient, which is $1/2 \sim 1/8$ approximately;

By calculating the average ambient wind speed at the typical height of 23 cities in China [9], the average wind speed at the typical height of 30, 50 and 100m in three fire protection fields was obtained. The boundary conditions for wind speed calculation were 0m/s without wind, 2m/s at low speed, 5m/s at medium speed and 10m/s at high speed.

2.2 Numerical Calculation Model

For the fire dynamics parameter settings, the unsteady-state heat release rate (HRR) of the bedroom was set to a baseline value of 6 MW, based on the distribution characteristics of combustible materials in the bedroom space and the technical standard GB 51251-2017 ("Technical Standard for Smoke Control Systems in Buildings") under conditions without sprinkler systems. Residential fires are typically unsteady-state fires, which can be described using the t^2 fire growth model.

$$Q = \alpha t^2 \quad (5)$$

Q is the heat release rate, kW; α is the fire growth coefficient, kW·s⁻²; t is the time after fire, s; The fire source material is wooden material [10], and the type of fire growth is rapid, so $\alpha = 0.044 \text{ kW} \cdot \text{s}^{-2}$, $t = 369\text{s}$ can be calculated by (5). The roof of the model is made of gypsum board [11], and the walls and ground are made of concrete [12]. The thermal and physical parameters of the two materials are shown in Table 2.

Three monitoring points were set up in the simulation for data acquisition to capture key parameter changes in the fire development process, with their specific parameters listed in Table 3.

As shown in Fig. 1, the monitoring sites are equipped with virtual sensors to record data on the loss rate, carbon monoxide concentration, and temperature change over time during the fire process. And the alarm threshold is shown in Table 4 below:

Table 2. Material Thermal Property Parameters

Materials	Density (kg/m ³)	Specific heat(kJ/(kg•K))	Thermal conductivity(W/(m•K))
Gypsum board	790	0.9	0.16
Concrete	2280	1.04	1.8

Table 3. Height Of Each Monitoring Point

Monitoring point	1	2	3
Height (m)	2.95	2.5	2

Table 4. Alarm Thresholds Of Monitoring Parameters

Name	Light Obscuration Rate	CO Concentration	Temperature
Alarm threshold	3.28%/m	50ppm	58°C

3 Results and Analysis

3.1 Light Obscuration Rate

Fig.2 illustrates the flow field and smoke distribution at the moment when the light obscuration rate reaches the alarm threshold under environmental wind speeds of 0 m/s, 2 m/s, 5 m/s, and 10 m/s. Comparing scenarios with and without wind, the presence of environmental wind enhances indoor convective flows. As wind speed increases, the turbulence intensity of the indoor flow field significantly intensifies, thereby influencing the movement and distribution of smoke within the space.

Fig. 3 shows the relationship between light obscuration rate and time at monitoring point 1. As illustrated, the light obscuration rate at this point exhibits a gradual increase during the early stage of the fire (<30 s), followed by a rapid rise to a stable fluctuation range. Under low environmental wind speeds (0 m/s and 2 m/s), the time required to reach the alarm threshold at all monitoring points is significantly shorter compared to high wind speeds (5 m/s and 10 m/s).

For monitoring point 1, the light obscuration rate curves for 0 m/s and 2 m/s are closely aligned, with alarm threshold times of 15.6 s and 20.1 s, respectively, differing by 4.5 s. This is attributed to the buoyancy-driven flow of high-temperature smoke, which has a lower density than the surrounding cold air. In contrast, at higher wind speeds (5 m/s and 10 m/s), the times to reach the threshold are 46.9 s and 90.7 s, respectively. This delay occurs because the driving force of the environmental wind dominates over the buoyancy force at higher speeds, causing a significant portion of the smoke to be carried away by the wind and resulting in a slower increase in light obscuration rate compared to low-speed conditions.

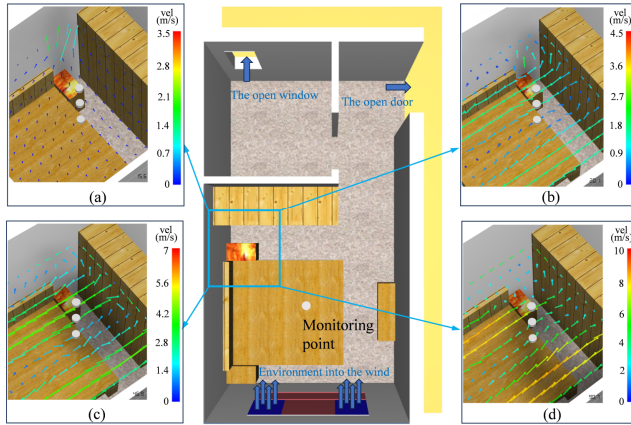


Fig. 2. Flow field and smoke distribution (a, Environment into the wind 0m/s; b, Environment into the wind 2m/s; c, Environment into the wind 5m/s; d, Environment into the wind 10m/s)

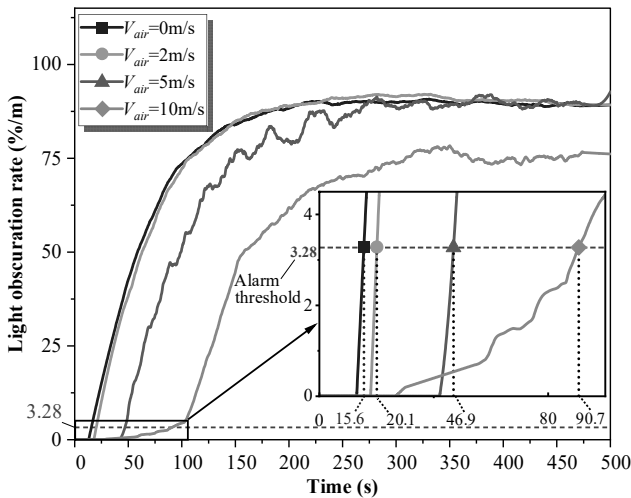


Fig. 3. Relation between dimming rate and time at monitoring point 1

Fig. 4 illustrates the relationship between environmental wind speed and the time required for the three monitoring points to reach the light obscuration rate alarm threshold. As shown, under low wind speeds (0 m/s and 2 m/s), the increase in time to reach the threshold is minimal. However, as the environmental wind speed increases, the time to reach the threshold increases significantly across all three monitoring points.

Compared to monitoring point 1, at wind speeds below 5 m/s, the time differences for monitoring points 2 and 3 to reach the threshold are more pronounced, but these differences diminish as wind speed increases. At wind speeds of 5 m/s or higher, the time

differences between the monitoring points become smaller and increase only gradually with further wind speed increases.

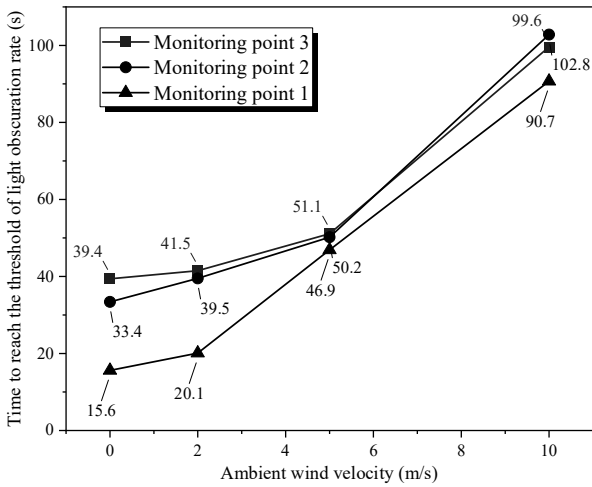


Fig. 4. Relationship between different monitoring points reaching the attenuation threshold and ambient wind speed

3.2 Temperature

Fig. 5 depicts the relationship between temperature and time at monitoring point 1. As shown, the temperature at this point exhibits an initial gradual increase, followed by a rapid rise to a stable fluctuation range as the fire develops. Under low environmental wind speeds (0 m/s and 2 m/s), the time required to reach the temperature alarm threshold is significantly shorter compared to high wind speeds (5 m/s and 10 m/s).

For monitoring point 1, Fig. 5 reveals distinct differences in the rate and magnitude of temperature rise under varying wind speeds. At 0 m/s, the temperature rises at the fastest rate and reaches the highest magnitude, resulting in the shortest time to reach the temperature alarm threshold. As the environmental wind speed increases, the rate of temperature rise decreases, the peak magnitude reduces, and the time to reach the threshold lengthens. This phenomenon is attributed to enhanced convective heat transfer at higher wind speeds, which increases heat transfer efficiency and allows more heat to be carried away by the environmental wind.

Fig. 6 illustrates the relationship between environmental wind speed and the time required for the three monitoring points to reach the temperature alarm threshold. As shown in Fig. 6, under low wind speeds (0 m/s and 2 m/s), the increase in time to reach the threshold is minimal. However, as the environmental wind speed increases, the time to reach the threshold increases significantly across all three monitoring points, while the time differences between them gradually decrease.

The rate of increase in time follows the order: monitoring point 1 > monitoring point 2 > monitoring point 3. This indicates that monitoring point 3 is the least affected by environmental wind speed, while monitoring point 1 is the most affected.

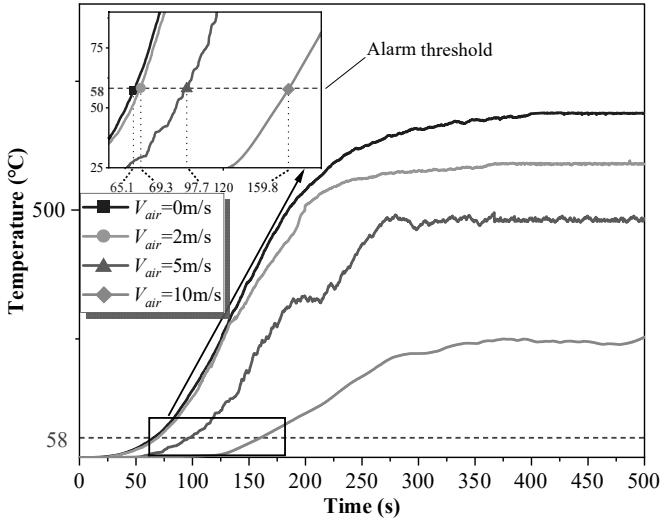


Fig. 5. Relation between temperature and time at monitoring point 1

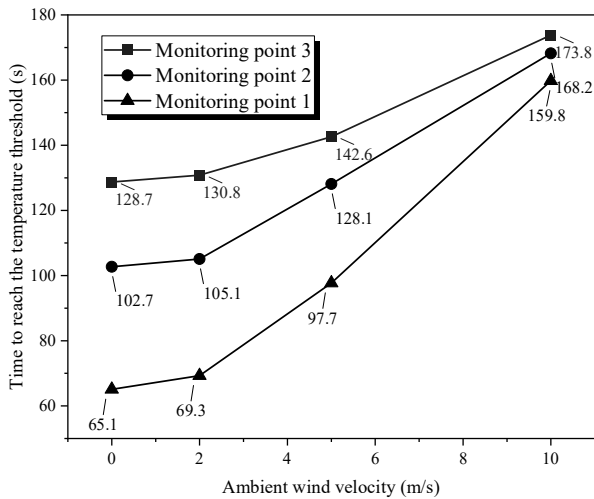


Fig. 6. Relation between the temperature threshold reached at 3 monitoring points and the ambient wind speed

3.3 CO Concentration

Fig.7 illustrates the relationship between CO concentration and time at monitoring point 1. As shown, the CO concentration at this point exhibits an initial gradual increase, followed by a rapid rise to a stable fluctuation range as the fire develops. Under low environmental wind speeds (0 m/s and 2 m/s), the time required to reach the CO concentration alarm threshold is significantly shorter compared to high wind speeds (5 m/s and 10 m/s).

For monitoring point 1, the CO concentration curves for 0 m/s and 2 m/s are closely aligned, with alarm threshold times of 58.7 s and 63.3 s, respectively, differing by 4.6 s. This is attributed to weaker air flow at lower wind speeds. At higher wind speeds (5 m/s and 10 m/s), the increased air flow rapidly disperses CO from the fire zone, reducing local CO concentration. Additionally, higher wind speeds enhance combustion efficiency, thereby reducing CO production from incomplete combustion.

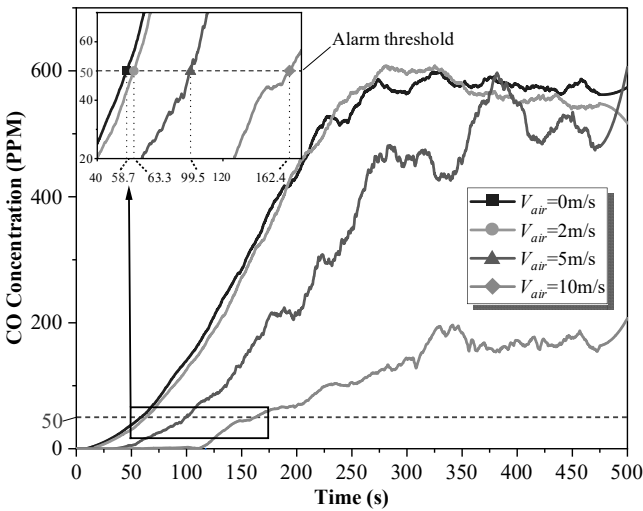


Fig. 7. Relationship between CO concentration at monitoring point 1 and time

Fig. 8 illustrates the relationship between environmental wind speed and the time required for the three monitoring points to reach the CO concentration alarm threshold. As shown, under low wind speeds (0 m/s and 2 m/s), the increase in time to reach the threshold is minimal. However, as the environmental wind speed increases, the time to reach the threshold increases significantly across all three monitoring points.

From the perspective of the monitoring points, Fig. 8, reveals that as the environmental wind speed increases, the time required for each monitoring point to reach the CO concentration threshold also increases. However, the time differences between the three monitoring points remain relatively constant.

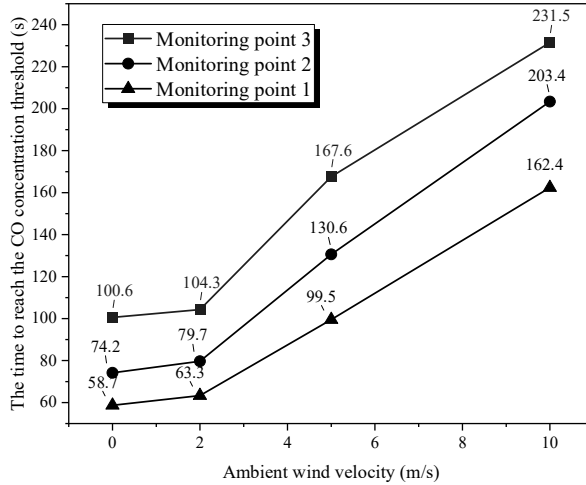


Fig. 8. Relation between CO concentration threshold at different monitoring points and ambient wind speed

4 Conclusions

This study employs FDS software to conduct numerical simulations of high-rise building fires, investigating the effects of environmental wind speed and monitoring height on fire alarm performance. The main conclusions are as follows:

(1) At lower environmental wind speeds (≤ 2 m/s), the increase in time to reach the alarm thresholds is minimal. Compared to no wind, the alarm times increase by approximately $0.29\times$, $0.06\times$, and $0.08\times$ for light obscuration rate, temperature, and CO concentration, respectively, indicating a limited impact on early warning performance. At higher environmental wind speeds, the time required for light obscuration rate, temperature, and CO concentration to reach their respective alarm thresholds increases significantly. Specifically, at 10 m/s compared to no wind, the alarm times increase by $4.8\times$, $1.45\times$, and $1.76\times$, respectively, resulting in a substantial reduction in early warning capability.

(2) At a monitoring height of 2.95 m, compared to 2.8 m and 2.5 m, the time required for light obscuration rate, temperature, and CO concentration to reach alarm thresholds is significantly reduced across all tested wind speeds (0 m/s, 2 m/s, 5 m/s, and 10 m/s), demonstrating a notable improvement in early warning capability.

(3) Due to the high average ambient wind of high-rise residential buildings, the early-warning ability of single-sensor fire alarm is unstable. More advanced detection technology can be integrated, so that the alarm threshold range can be automatically adjusted according to the change of environmental wind speed, and then multi-sensor fusion combined with visual recognition can improve the early warning ability and reliability under the influence of wind speed.

Acknowledgments

This work was financially supported by the Talent Introduction Project of Sichuan University of Science & Engineering (2019RC18), the Key Laboratory of Process Equipment and Control Engineering in Colleges and Universities of Sichuan Province (GK201910), and the 2024 Luzhou Science and Technology Program Projects (2024SYF183). Additionally, it was supported by the Scientific Research and Innovation Team Program of Sichuan University of Science & Engineering (SUSE652A004) and Yibin city science and technology plan project (2023SF007).

References

1. L. Jianlin, F. Libi, and S. Yonggan, "Safety evacuation design and optimization of high-rise residential buildings," *Journal of Fuzhou University (Natural Science Edition)*, vol. 49, no. 1, pp. 115–120, 2021.(in Chinese)
2. Y. Hang, J. Yaqiang, H. Qinli, and T. Longfei, "Environmental wind speed design of fire experiment of high-rise building," *Fire Science and Technology*, no. 9, pp. 1225–1228, 2019.(in Chinese)
3. H. Song, Y. Shi, H. Yao, X. Wei, H. Qin, Z. Lou, and Y. Yu, "Influence of wind direction on fire spread on high-rise building facades," *Fire*, vol. 7, no. 11, p. 384, 2024.
4. S. Yang, Y. Li, Z. Su, and J. Li, "Study on the fire spread characteristics of high-rise building facades under strong wind conditions based on the combination of WRF and CFD," *Applied Sciences*, vol. 15, no. 3, p. 1327, 2025.
5. J. He, Y. Sheng, X. Wu, and J. Wang, "Influence of external wind on fire characteristics and smoke dynamics in a stairwell adjacent to a room," *Case Studies in Thermal Engineering*, vol. 60, p. 104644, 2024.
6. R. Gao, Z. Fang, A. Li, C. Shi, and L. Che, "Estimation of building ventilation on the heat release rate of fire in a room," *Applied Thermal Engineering*, vol. 121, pp. 1111–1116, 2017.
7. M. Liu and G. Wang, "Indoor fire simulation in low-rise teaching buildings based on BIM–FDS," *Fire*, vol. 6, no. 5, p. 203, 2023.
8. N. Meng, L. Hu, L. Wu, L. Yang, S. Zhu, L. Chen, and W. Tang, "Numerical study on the optimization of smoke ventilation mode at the conjunction area between tunnel track and platform in emergency of a train fire at subway station," *Tunnelling and Underground Space Technology*, vol. 40, pp. 151–159, 2014.
9. D. Ling and H. Zheng, "Influence of environmental wind speed on natural smoke exhaust in vestibule," *Fire Science and Technology*, vol. 39, no. 7, pp. 931–934, 2020.(in Chinese)
10. M. J. Hurley, D. T. Gottuk, J. R. Hall Jr, K. Harada, E. D. Kuligowski, M. Puchovsky, J. M. Watts Jr, and C. J. Wiecezorek, *SFPE Handbook of fire protection engineering*. Springer, 2016, pp. 1143–1232.
11. R. Wasson, M. N. Nahid, B. Y. Lattimer, and T. E. Diller, "Influence of a ceiling on fire plume velocity and temperature," *Fire Technology*, vol. 52, no. 6, pp. 1863–1886, 2016.
12. K. McGrattan, S. Hostikka, R. McDermott, J. Floyd, M. Vanella, C. Weinschenk, and K. Overholt, *Fire dynamics simulator (version 6.6.0), User's guide*, 6th ed. Gaithersburg, MD: National Institute of Standards and Technology, 2017, pp. 31, 41.

Open Access This chapter is licensed under the terms of the Creative Commons Attribution-NonCommercial 4.0 International License (<http://creativecommons.org/licenses/by-nc/4.0/>), which permits any noncommercial use, sharing, adaptation, distribution and reproduction in any medium or format, as long as you give appropriate credit to the original author(s) and the source, provide a link to the Creative Commons license and indicate if changes were made.

The images or other third party material in this chapter are included in the chapter's Creative Commons license, unless indicated otherwise in a credit line to the material. If material is not included in the chapter's Creative Commons license and your intended use is not permitted by statutory regulation or exceeds the permitted use, you will need to obtain permission directly from the copyright holder.

